nature nanotechnology

LETTERS

https://doi.org/10.1038/s41565-019-0620-x

Single-molecule tautomerization tracking through space- and time-resolved fluorescence spectroscopy

Benjamin Doppagne[1], Tomáš Neuman[2], Ruben Soria-Martinez[1], Luis E. Parra López[1], Hervé Bulou[1], Michelangelo Romeo[1], Stéphane Berciaud[1], Fabrice Scheurer[1], Javier Aizpurua[2] and Guillaume Schull[1*]

Tautomerization, the interconversion between two constitutional molecular isomers, is ubiquitous in nature[1], plays a major role in chemistry[2] and is perceived as an ideal switch function for emerging molecular-scale devices[3]. Within free-base porphyrin[4], porphycene[5] or phthalocyanine[6], this process involves the concerted or sequential hopping of the two inner hydrogen atoms between equivalent nitrogen sites of the molecular cavity. Electronic and vibronic changes[6] that result from this NH tautomerization, as well as details of the switching mechanism, were extensively studied with optical spectroscopies, even with single-molecule sensitivity[7]. The influence of atomic-scale variations of the molecular environment and submolecular spatial resolution of the tautomerization could only be investigated using scanning probe microscopes[3,8–11], at the expense of detailed information provided by optical spectroscopies. Here, we combine these two approaches, scanning tunnelling microscopy (STM) and fluorescence spectroscopy[12–15], to study the tautomerization within individual free-base phthalocyanine (H_2Pc) molecules deposited on a NaCl-covered Ag(111) single-crystal surface. STM-induced fluorescence (STM-F) spectra exhibit duplicate features that we assign to the emission of the two molecular tautomers. We support this interpretation by comparing hyper-resolved fluorescence maps[15–18](HRFMs) of the different spectral contributions with simulations that account for the interaction between molecular excitons and picocavity plasmons[19]. We identify the orientation of the molecular optical dipoles, determine the vibronic fingerprint of the tautomers and probe the influence of minute changes in their atomic-scale environment. Time-correlated fluorescence measurements allow us to monitor the tautomerization events and to associate the proton dynamics to a switching two-level system. Finally, optical spectra acquired with the tip located at a nanometre-scale distance from the molecule show that the tautomerization reaction occurs even when the tunnelling current does not pass through the molecule. Together with other observations, this remote excitation indicates that the excited state of the molecule is involved in the tautomerization reaction path.

A sketch of the experiment is given in Fig. 1a, which shows the silver-covered tungsten tip of a cryogenic STM used to excite the fluorescence of a single H_2Pc molecule (Fig. 1b) deposited on Ag(111) covered by three layers of NaCl. A differential conductance (dI/dV) spectrum (Fig. 1c) recorded on a H_2Pc molecule reveals the energy positions of the highest occupied and lowest unoccupied molecular orbitals ($E_{HOMO} \approx -2.5$ eV and $E_{LUMO} \approx 0.7$ eV (HOMO, highest occupied molecular orbital; LUMO, lowest unoccupied molecular orbital)). This assignment was confirmed by STM images recorded at the energies of the two spectral contributions (Fig. 1d,e), which can be directly compared to density functional theory calculations of the spatial projections of the HOMO and LUMO of H_2Pc (Supplementary Section 1). The LUMO may exhibit two similar twofold symmetry patterns (Fig. 1d), rotated by 90°, which can be assigned[20] to the two different tautomers (Fig. 1b). For a given molecule, a change of the pattern is often observed after a scan of the molecule at a negative voltage. The HOMO, however, always reveals the same fourfold symmetry image. STM-F spectra recorded at a negative voltage ($V = -2.5$ V) for three different positions (1, 2 and 3 in Fig. 1e) of the STM tip with respect to the H_2Pc molecule are displayed in Fig. 1f. The spectrum for position 1 (red line) shows an intense emission peak at 1.80 eV, a weaker peak at 1.92 eV and a series of very weak vibronic features on the low energy side of the main peaks. Based on a comparison with the literature[6,14], the peaks at 1.80 eV and 1.92 eV can be assigned to the two first optical transitions of the H_2Pc molecule named Q_x and Q_y, respectively. Q_x and Q_y correspond to transition dipole moments oriented along and perpendicularly, respectively, to the two inner hydrogen atoms of H_2Pc. The spectrum acquired on the same molecule in position 3 (Fig. 1f) shows a very similar spectral structure, but with a 20 meV shift of the Q_x peak to higher energies. Eventually, the spectrum for position 2 acquired in-between two benzopyrrole units of the H_2Pc molecule shows that this shift results from a duplication of the main spectral feature. Fluorescence spectra that exhibit a reduced energy separation between the duplicated peaks or no separation at all were also recorded for other H_2Pc molecules. The presence or absence of duplicate features in the spectra results from minute changes in the environment of the H_2Pc molecules caused by their adsorption on different sites of the NaCl/Ag(111) Moiré pattern[21] (details in Supplementary Section 2).

To unveil a potential connection between the duplicate spectra and the presence of two different tautomers, we acquired HRFMs of the molecule. We recorded a grid of STM-F spectra following an already developed approach[15–18]. A HRFM shows the spatial variation of the photon intensity associated with a given spectral feature

[1]Université de Strasbourg, CNRS, IPCMS, UMR 7504, Strasbourg, France. [2]Center for Materials Physics (CSIC-UPV/EHU) and DIPC, Donostia-San Sebastián, Spain. *e-mail: guillaume.schull@ipcms.unistra.fr

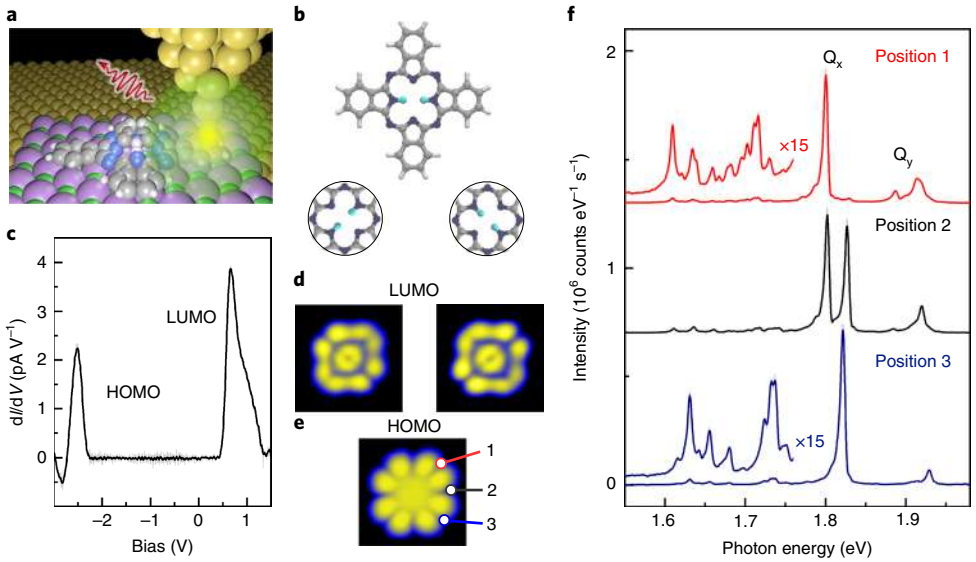

Fig. 1 | STM-F spectroscopy of individual H_2Pc molecules. a, Sketch of the STM-induced emission experiment. **b**, Ball-and-stick model of the free-base phthalocyanine (H_2Pc) and zoom on the central part of the molecule to highlight the structure of the two tautomers. **c**, dI/dV spectrum acquired on a single H_2Pc adsorbed on three layers of NaCl on Ag(111). **d**,**e**, STM images (3 × 3 nm^2, I = 10 pA) acquired at V = 0.55 V (**d**) and V = −2.5 V (**e**). Two patterns tilted by 90° from each other can be observed in the image of a same molecule recorded at V = 0.55 V (**d**) and correspond to the two tautomers. **f**, STM-F spectra acquired (V = −2.5 V, I = 100 pA, acquisition time t = 120 s) for the STM tip located at the positions identified in **e**.

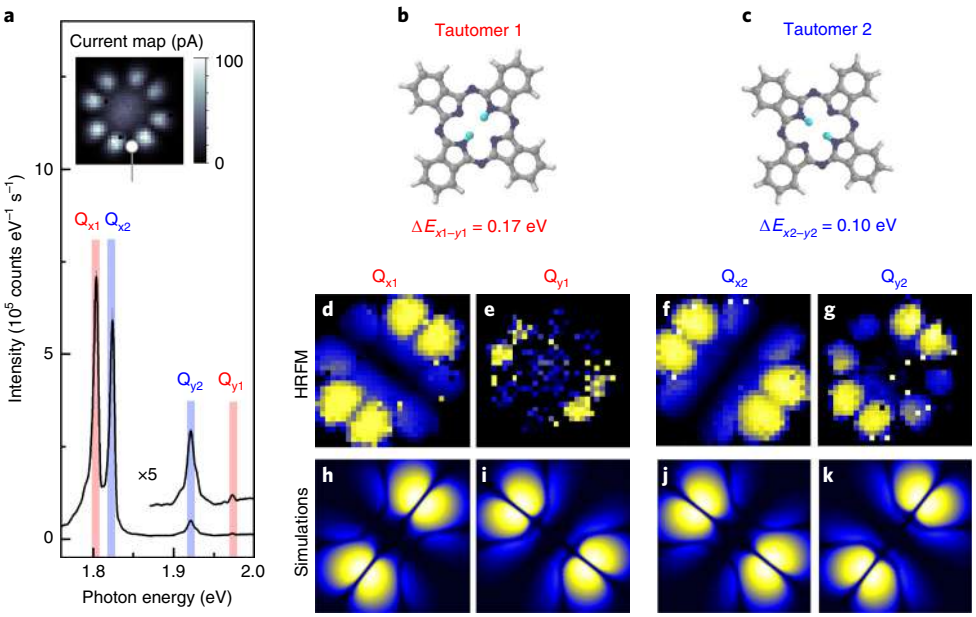

Fig. 2 | Highly resolved fluorescence mapping of a single H_2Pc molecule. a, STM-F spectrum (V = −2.5 V, I = 100 pA, acquisition time t = 180 s) acquired at the position marked by a white disk in the current image (2.5 × 2.5 nm^2, V = −2.5 V) in the inset. **b**–**k**, The chemical structure of tautomers 1 (**b**) and 2 (**c**) from the associated HRFMs (**d**–**g**) (2.5 × 2.5 nm^2, acquired simultaneously with the current map in **a**, acquisition time t = 50 s pixel^{-1}, 30 × 30 pixels), and from their related simulated maps for the main contributions (Q_{x1}, Q_{x2}, Q_{y1} and Q_{y2}) (**h**–**k**) identified in **a**. Photon energy integration intervals were $1.798 < h\nu < 1.811$ eV (**d**), $1.972 < h\nu < 1.981$ eV (**e**), $1.824 < h\nu < 1.832$ eV (**f**) and $1.923 < h\nu < 1.941$ eV (**g**).

with submolecular spatial resolution. The HRFMs were acquired with a constant tip–sample separation (that is, open feedback loop) to prevent distance-related artefacts and are normalized by the tunnelling current to have constant excitation intensities (Methods). In Fig. 2b,c, we display the HRFMs of four light-emission contributions, Q_{x1}, Q_{x2}, Q_{y1} and Q_{y2}, in the spectrum of Fig. 2a. All the HRFMs show bright features on two opposite sides of the molecule that are separated by a darker region. Superimposed on these bright and dark regions, we also identify features that are reminiscent of the HOMO pattern (Supplementary Section 1). In Fig. 2b,c, we also display theoretical simulations of the HRFMs characteristic of the Q_x and Q_y transition dipole moments of the H_2Pc molecule. These simulations estimate the current-normalized fluorescence intensity for a given tip position by accounting for the product of the

probability to drive the molecule in an excited state and the probability for this excitation to decay radiatively (details in Supplementary Section 3). Our simulations confirm that the excitation efficiency is larger when electron tunnelling takes place through the HOMO. This is in agreement with the increased fluorescence intensity observed when the bias is driven to resonance with the HOMO of the molecule[14]. This is also compatible with both the recent many-body state description of the excitation mechanism proposed by Miwa et al. that involves a charging step of the molecule by electron removal from the HOMO[22], and an enhanced energy transfer between a tunnelling electron and a molecular exciton[13,18,23] that would occur for voltages driven at resonance with the HOMO. The radiative decay probability, however, is estimated by following a method described in detail in Neuman et al.[24] by calculating the coupling strength between the picocavity plasmons[19], that is, the electromagnetic modes confined to an atomic-scale volume at the apex of the plasmonic tip, and the Q_x and Q_y transition dipole moments of H_2Pc. As observed previously[15,16,25], this coupling results in an increased (attenuated) emission intensity for the tip localized at the extremities (centre) of the molecular dipoles. In our case, the extreme spatial localization of the field is responsible for the close to atomic-scale spatial resolution in the fluorescence maps. The excellent agreement between experimental and theoretical maps suggests that two series of Q_x and Q_y contributions correspond to the two tautomers of the H_2Pc molecules.

To emit at different energies, the two tautomers, which are otherwise equivalent, must experience slightly different environments[6,26]. This is confirmed by the substantially different Q_x–Q_y gaps of the two tautomers. Although this gap is pretty close to that observed in cryogenic matrices[6] for tautomer 2, it is much larger for tautomer 1. This environment difference also affects the vibronic spectra (spectra 1 (blue) and 3 (red) in Fig. 1f). A detailed comparison of these vibronic fingerprints with a Raman spectrum obtained on a macroscopic crystal of H_2Pc (Supplementary Section 4) confirms that tautomer 2 is weakly affected by its adsorption site, whereas the geometry of tautomer 1 is probably strained. This interpretation is supported by time-dependent density functional theory calculations of the H_2Pc molecule that reveal similar variations of the Q_x–Q_y gap for an artificial compression (tension) of 5% (10%) of the molecule size along the Q_x axis (Q_y axis) (Supplementary Section 5). This combined spatial and spectral optical approach allows us to identify minute changes in the electronic structure and the geometry of the two conformers that cannot be measured separately. The NaCl/Ag(111) Moiré pattern (Supplementary Section 2) is probably responsible for this small variation in the tautomer environments.

Assigning the spectral contributions to two different tautomers also implies a fast switching of the molecule between these two conformations during the acquisition of the spectra and the HRFMs. To track the tautomerization dynamics directly through the STM-F spectra, we separated the collected light in two paths filtered at the energies of the Q_{x1} and Q_{x2} contributions, respectively, and eventually funnelled to avalanche photodiodes (APDs) having a dead time of ~100 ns (Fig. 3a). In Fig. 3b, we display 200 ms of the time traces of the Q_{x1} and Q_{x2} emission lines (Fig. 3c) recorded simultaneously with the tunnelling current. These traces reveal alternating intense and weak emission periods for the two light contributions. Besides, the two traces seem to be complementary, that is, Q_{x1} is intense when Q_{x2} is weak and vice versa. Eventually, we note that these variations match fluctuations observed in the tunnelling current that could then be assigned to changes of the local conductance for the two tautomers.

To confirm and quantify these observations, we follow a fluorescence correlation spectroscopy approach[27] that was recently used in combination with STM to characterize molecular fluctuations[28,29] and single-photon sources[30,31]. We display in Fig. 3d the second-order autocorrelation functions $g_{ii}^{(2)}(\tau) = \langle I_{Q_{xi}}(\tau) I_{Q_{xi}}(t+\tau)\rangle / \langle I_{Q_{xi}}(t)\rangle^2$ and the second-order cross-correlation function $g_{12}^{(2)}(\tau) = \langle I_{Q_{x1}}(\tau) I_{Q_{x2}}(t+\tau)\rangle / \langle I_{Q_{x1}}(t)\rangle \langle I_{Q_{x2}}(t)\rangle$ of the fluorescence intensity ($I_{Q_{xi}}$) of the Q_{x1} and Q_{x2} contributions. The $g_{11}^{(2)}(\tau)$ and $g_{22}^{(2)}(\tau)$ functions allow us to estimate the probability of observing successive photons[27] separated by a time τ on APD 1 and 2, respectively, whereas the $g_{12}^{(2)}(\tau)$ function characterizes the probability to detect a Q_{x2} photon at a time τ after the detection of a Q_{x1} photon. For short time separations, the autocorrelation functions reveal a bunched emission ($g_{ii}^{(2)}(\tau) > 1$), whereas antibunching is evidenced in the cross-correlation function ($g_{12}^{(2)}(\tau) < 1$). For larger values of τ, an uncorrelated emission ($g^{(2)}(\tau) = 1$) characterizes both functions. Several conclusions may be drawn from these results. The presence of antibunching in the $g_{12}^{(2)}(\tau)$ function confirms that the Q_{x1} and Q_{x2} contributions belong to two configurations that do not appear at the same time, which thus validates the hypothesis of a switching between the two tautomeric forms. The bunching observed in $g_{ii}^{(2)}(\tau)$ supports this interpretation and directly reflects the presence of time laps during which the molecule remains in a given tautomer. Moreover, we deduce from tip-position dependent correlation measurements that the time spent by the molecule in the tautomer 2 configuration is consistently longer than that in the tautomer 1 configuration (Supplementary Section 6), which agrees well with the more stable character of the tautomer 2 configuration. The $g_{ii}^{(2)}$ functions can be very well fitted with a single exponential decay, $g_{ii}^{(2)}(\tau) = 1 + A\ \exp(-k\tau)$ where k is the tautomer switching frequency[27]. We show in Fig. 3e that the dependency of k with tunnelling current is slightly superlinear. This is somehow surprising in the frame of the electron-activated process generally considered in this case[3]. Besides, we see (Fig. 3e) that the tautomerization rate follows almost the same current dependency as the fluorescence intensity. Interestingly, a similar correlation exists between the voltage dependencies of these two processes. Indeed, a reduction of the switching rate is observed in current traces recorded at lower absolute voltages (Fig. 4a), and is beyond detection for voltages ≥ -1.7 V. It is at this same voltage threshold that we start to observe (Fig. 4b) the fluorescence of the molecule. This correlation may indicate an activation mechanism in which the tautomerization reaction occurs through an excitation/de-excitation cycle of the molecule. To possibly identify such an effect, we recorded fluorescence spectra for the same voltage sequence (Fig. 4c), but with the tip located ~1.2 nm laterally away from the molecule (STM image in the inset of Fig. 4c). In this configuration, it has been shown that the molecule can still be driven to its excited state through energy transfer between the tunnelling electron and the molecular exciton[20,25,32]. In contrast, processes directly activated by tunnelling electrons that traverse the molecule, such as charging[33], cannot occur. The data in Fig. 4c show that both Q_{x1} and Q_{x2} contributions are observed in all the spectra acquired with $V < -1.8$ eV, which implies that the tautomerization occurs even in the absence of direct tunnelling through the molecule. Together with the current (Fig. 3e) and voltage (Fig. 4a) dependencies, this indicates an excited-state proton transfer, similar to that deduced from laser-excitation experiments[34]. This conclusion is further supported by similar data acquired on single free-base naphthalocyanine molecules that have a lower optical gap and consequently revealed a tautomerization onset at a lower voltage (Supplementary Section 7). As fluorescence information was not available, this mechanism was not considered in previous tautomerization experiments induced by STM[3,8,10,35,36] (Supplementary Section 7 gives a detailed discussion of the tautomerization mechanism). This mechanism may also be involved in other STM-activated phenomena, such as diffusion, rotation, dissociation or the switching of single molecules on the surface.

We used hyper-resolved fluorescence microscopy in combination with time-correlated measurements and spectral selection to identify and characterize a tautomerization reaction within a

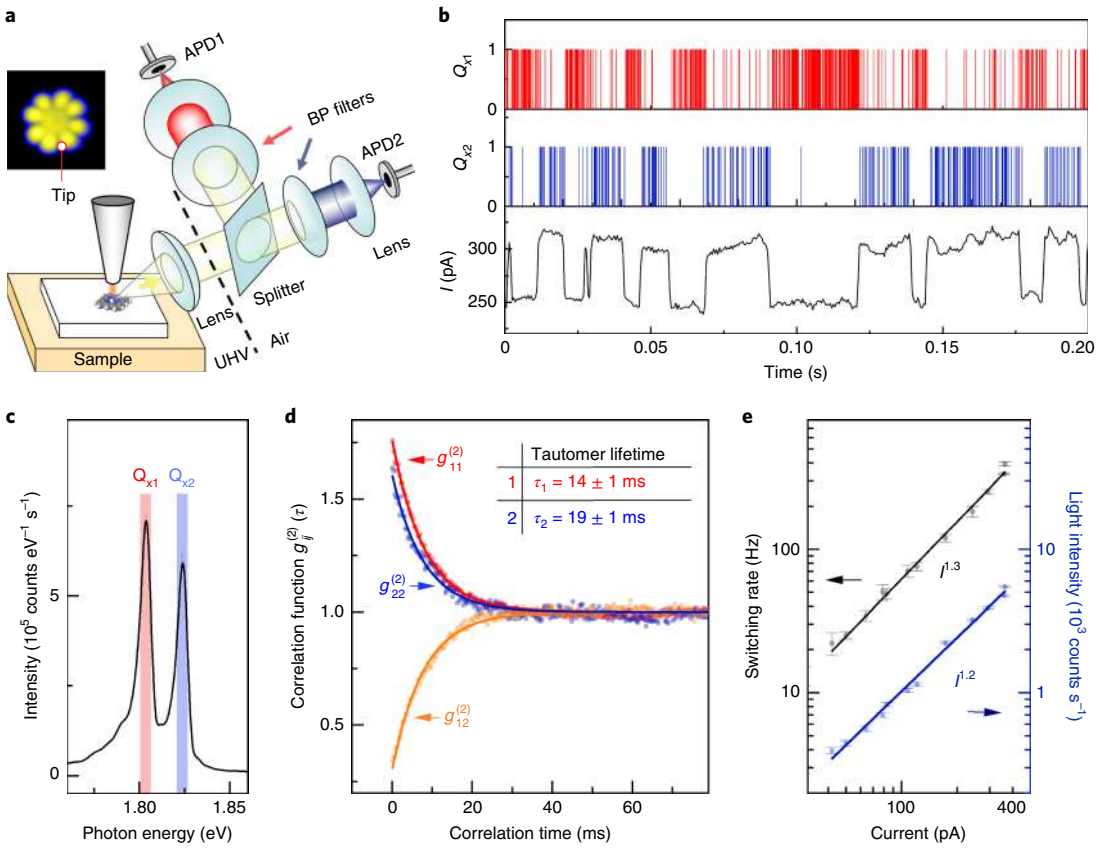

Fig. 3 | Tautomerization dynamics revealed by spectrally filtered time-correlated fluorescence. a, Sketch of the time-resolved set-up. STM image of the molecule (V = -2.5 V, I = 10 pA, 3.5 × 3.5 nm^2). **b**, Time traces of the signal recorded simultaneously on APD1 and APD2, which correspond to the Q_{x1} and Q_{x2} contributions, respectively, and of the tunnel current (V = -2.5 V). The tip position is indicated by a dot in the STM image in **a**. **c**, For this position of the tip, STM-F spectra display intense Q_{x1} and Q_{x2} contributions. **d**, Second-order autocorrelation ($g^{(2)}_{ii}$) and cross-correlation function ($g^{(2)}_{ij}$) of the signal measured by the APDs. **e**, Plot of the switching rate k as deduced from fits of the $g^{(2)}$ functions and of the light intensity (for V = -2.5 V) as a function of the tunnelling current. Errors are estimated by accounting for the standard deviation of the averaged light intensity in the bright and dark states of the APD1 and APD2 time traces and the error on the linear fit applied to the correlation functions in a logarithmic scale. BP, bandpass; UHV, ultrahigh vacuum.

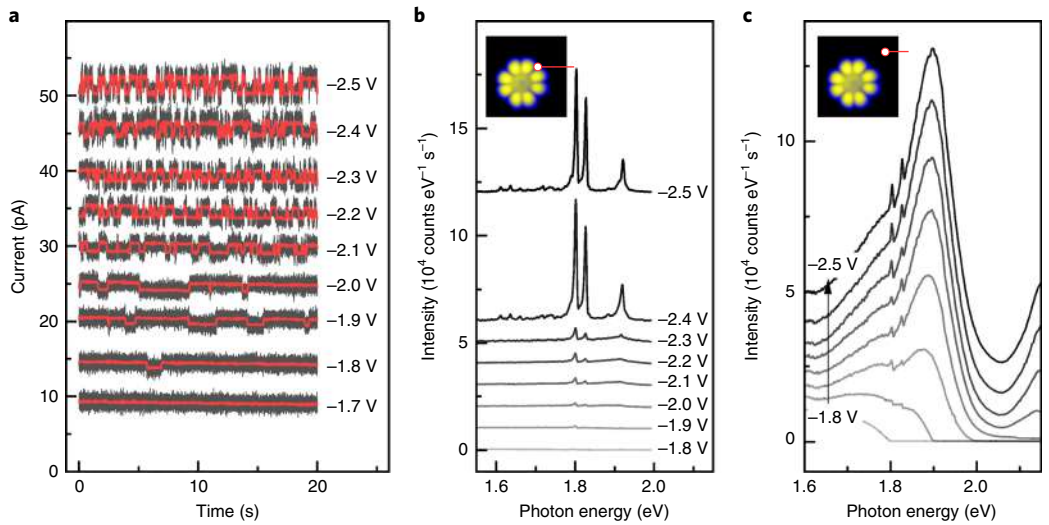

Fig. 4 | Excited-state mediated tautomerization reaction. a–**c**, Current–time traces (initial setpoint I = 10 pA) (**a**) and STM-F spectra (I = 10 pA (**b**) and I = 600 pA (**c**)) as a function of V. Current traces and spectra are vertically offset for clarity. The position of the tip in **a** and **b** is marked by a dot in the STM image (V = -2.5 V, I = 10 pA, 4 × 4 nm^2) in the inset of **b** (the tip position is similarly shown in the inset of **c**).

prototypical single-molecule switch. We obtained detailed information on the interaction of the molecule and the substrate in the two tautomeric conformations, on the dynamics of the hydrogen atoms within the molecule and on the activation mechanism of the reaction in the STM junction. We believe that the unravelled reaction path, which involves the excited state of the molecule, may also

play an important role in several other STM-activated experiments for which it has not been considered. Moreover, by developing a simulation method that accounts for both the excitation and de-excitation probabilities in a STM-F experiment, in which molecular switches are shown to modulate only the current traversing a nanoscale circuit, we demonstrate that a molecular optoelectronic element can also be used to activate an optical signal.

Online content

Any methods, additional references, Nature Research reporting summaries, source data, extended data, supplementary information, acknowledgements, peer review information; details of author contributions and competing interests; and statements of data and code availability are available at https://doi.org/10.1038/s41565-019-0620-x.

Received: 18 July 2019; Accepted: 9 December 2019;
Published online: 20 January 2020

References

1. Abou-Zied, O. K., Jimenez, R. & Romesberg, F. E. Tautomerization dynamics of a model base pair in DNA. *J. Am. Chem. Soc.* **123**, 4613–4614 (2001).
2. Antonov, L. Tautomerism—Methods and Theories (Wiley, 2014).
3. Liljeroth, P., Repp, J. & Meyer, G. Current-induced hydrogen tautomerization and conductance switching of naphthalocyanine molecules. *Science* **317**, 1203–1206 (2007).
4. Storm, C. B. & Teklu, Y. Nitrogen–hydrogen tautomerism in porphyrines and chlorines. *J. Am. Chem. Soc.* **94**, 1745–1747 (1972).
5. Waluk, J. Spectroscopy and tautomerization studies of porphycenes. *Chem. Rev.* **117**, 2447–2480 (2017).
6. Murray, C. et al. Visible luminescence spectroscopy of free-base and zinc phthalocyanines isolated in cryogenic matrices. *Phys. Chem. Chem. Phys.* **13**, 17543–17554 (2011).
7. Chizhik, A. M. et al. Optical imaging of excited-state tautomerization in single molecules. *Phys. Chem. Chem. Phys.* **13**, 1722–1733 (2011).
8. Kumagai, T. et al. Thermally and vibrationally induced tautomerization of single porphycene molecules on a Cu(110) surface. *Phys. Rev. Lett.* **111**, 246101 (2013).
9. Kumagai, T. et al. Controlling intramolecular hydrogen transfer in a porphycene molecule with single atoms or molecules located nearby. *Nat. Chem.* **6**, 41–46 (2013).
10. Ladenthin, J. N. et al. Force-induced tautomerization in a single molecule. *Nat. Chem.* **8**, 935–940 (2016).
11. Kügel, J., Klein, L., Leisegang, M. & Bode, M. Analyzing and tuning the energetic landscape of H_2Pc tautomerization. *J. Phys. Chem. C* **121**, 28204–28210 (2017).
12. Qiu, X. H., Nazin, G. V. & Ho, W. Vibrationally resolved fluorescence excited with submolecular precision. *Science* **299**, 542–546 (2003).
13. Chong, M. C. et al. Narrow-line single-molecule transducer between electronic circuits and surface plasmons. *Phys. Rev. Lett.* **116**, 036802 (2016).
14. Imada, H. et al. Real-space investigation of energy transfer in heterogeneous molecular dimers. *Nature* **538**, 364–367 (2016).
15. Zhang, Y. et al. Visualizing coherent intermolecular dipole–dipole coupling in real space. *Nature* **531**, 623–627 (2016).
16. Chen, C., Chu, P., Bobisch, C. A., Mills, D. L. & Ho, W. Viewing the interior of a single molecule: vibronically resolved photon imaging at submolecular resolution. *Phys. Rev. Lett.* **105**, 217402 (2010).
17. Lee, J., Perdue, S. M., Perez, A. R. & Apkarian, V. A. Vibronic motion with joint Angstrom–femtosecond resolution observed through Fano progressions recorded within one molecule. *ACS Nano* **8**, 54–63 (2014).
18. Doppagne, B. et al. Vibronic spectroscopy with submolecular resolution from STM-induced electroluminescence. *Phys. Rev. Lett.* **118**, 127401 (2017).
19. Urbieta, M. et al. Atomic-scale lightning rod effect in plasmonic picocavities: a classical view to a quantum effect. *ACS Nano* **12**, 585–595 (2018).
20. Imada, H. et al. Single-molecule investigation of energy dynamics in a coupled plasmon–exciton system. *Phys. Rev. Lett.* **119**, 013901 (2017).
21. Pivetta, M., Patthey, F., Stengel, M., Baldereschi, A. & Schneider, W.-D. Local work function Moiré pattern on ultrathin ionic films: NaCl on Ag(100). *Phys. Rev. B* **72**, 115404 (2005).
22. Miwa, K. et al. Many-body state description of single-molecule electroluminescence driven by a scanning tunneling microscope. *Nano Lett.* **19**, 2803–2811 (2019).
23. Chong, M. C. et al. Ordinary and hot electroluminescence from single-molecule devices: controlling the emission color by chemical engineering. *Nano Lett.* **16**, 6480–6484 (2016).
24. Neuman, T., Esteban, R., Casanova, D., García-Vidal, F. J. & Aizpurua, J. Coupling of molecular emitters and plasmonic cavities beyond the point-dipole approximation. *Nano Lett.* **18**, 2358–2364 (2018).
25. Kröger, J., Doppagne, B., Scheurer, F. & Schull, G. Fano description of single-hydrocarbon fluorescence excited by a scanning tunneling microscope. *Nano Lett.* **18**, 3407–3413 (2018).
26. Macfarlane, R. & Völker, S. A comparison of phototautomerism in different sites of free-base porphin (H_2P) in *n*-alkane crystals. *Chem. Phys. Lett.* **69**, 151–155 (1980).
27. Lippitz, M., Kulzer, F. & Orrit, M. Statistical evaluation of single nano-object fluorescence. *ChemPhysChem* **6**, 770–789 (2005).
28. Perronet, K., Schull, G., Raimond, P. & Charra, F. Single-molecule fluctuations in a tunnel junction: a study by scanning-tunnelling-microscopy-induced luminescence. *Europhys. Lett.* **74**, 313–319 (2006).
29. Merino, P. et al. A single hydrogen molecule as an intensity chopper in an electrically driven plasmonic nanocavity. *Nano Lett.* **19**, 235–241 (2019).
30. Merino, P., Große, C., Rosławska, A., Kuhnke, K. & Kern, K. Exciton dynamics of C_{60}-based single-photon emitters explored by Hanbury Brown-Twiss scanning tunnelling microscopy. *Nat. Commun.* **6**, 8461 (2015).
31. Zhang, L. et al. Electrically driven single-photon emission from an isolated single molecule. *Nat. Commun.* **8**, 580 (2017).
32. Zhang, Y. et al. Sub-nanometre control of the coherent interaction between a single molecule and a plasmonic nanocavity. *Nat. Commun.* **8**, 15225 (2017).
33. Doppagne, B. et al. Electrofluorochromism at the single-molecule level. *Science* **361**, 251–255 (2018).
34. Völker, S. & van der Waals, J. Laser-induced photochemical isomerization of free base porphyrin in an *n*-octane crystal at 4.2 K. *Mol. Phys.* **32**, 1703–1718 (1976).
35. Kügel, J. et al. Remote single-molecule switching: identification and nanoengineering of hot electron-induced tautomerization. *Nano Lett.* **17**, 5106–5112 (2017).
36. Böckmann, H. et al. Near-field enhanced photochemistry of single molecules in a scanning tunneling microscope junction. *Nano Lett.* **18**, 152–157 (2018).

Methods

The experiments were performed with a low-temperature (4.5 K) Omicron STM operating under a ultrahigh vacuum. The microscope was complemented with an optical set-up capable of detecting the light emitted at the tip–sample junction. The emitted photons were collected with a lens located in the vacuum chamber at 4.5 K and then transferred out of the chamber. To characterize the spectral dependency of the emitted light and the HRFMs, the light was focused on an optical fibre that was connected to a spectrograph coupled to a charge-coupled device camera. Two optical gratings of 300 and 1,200 grooves were used, which resulted in spectral resolutions of ~0.7 nm (spectra in Figs. 1–4 and Supplementary Figs. 6, 11, 12 and 13) and 0.2 nm (spectra of Supplementary Figs. 2 and 3) respectively. The details of the optical set-up are described in the Supplemental Material of Chong et al.[13]. For the time-resolved measurements (Fig. 3a) the photon stream was divided into two lines by a 50/50 splitter, filtered using bandpass filters (bandwidth of 10 nm centred at 676 and 690 nm) and eventually focused on two APDs (Excelitas SPCM-AGRH-FC). The STM tips were prepared from electrochemically etched tungsten wire. In situ, they were prepared by Ar^+ sputtering and annealing. The tips were eventually indented in the sample to cover them with a thin silver layer to optimize their plasmonic response. The Ag(111) substrates were cleaned by several sputtering and annealing cycles. NaCl was evaporated on the Ag(111) sample, which was held at around 300 K. The molecules were deposited on the sample at a low temperature (~10 K) from a powder placed in a quartz crucible. The Raman spectra (Supplementary Fig. 6b) were acquired at resonance on a H_2Pc crystal at room temperature and in air (excitation wavelength, 632.8 nm). HRFMs were generated by scanning the targeted molecule with the STM tip while recording a STM-F spectrum for each tip position (that is, pixel of the map). The tip–molecule separation was kept constant during the acquisition (open feedback loop) to prevent any distance-related artefacts. To compensate for drifts of the tip during the long acquisition of the HRFMs, the (x,y,z) position of the tip was corrected using an 'atom-tracking' procedure between the acquisition of each pixel, similarly to the procedure developed in Kawai et al.[37]. The next step consists of choosing the photon energy windows that correspond to the spectral feature of interest, namely, Q_{x1}, Q_{x2}, Q_{y1} and Q_{y2}, to generate the corresponding photon intensity maps. By this method, all the HRFMs were recorded simultaneously in a single experimental run and readily compared. Eventually, the photon intensity maps were normalized by the STM current map recorded simultaneously. Indeed, as the tunnelling current acts in this experiment as an excitation source and as the current varies as a function of tip position, normalizing for each pixel the photon intensity by the corresponding tunnelling current allows us to generate maps with a constant excitation source intensity.

Data availability

The data that support the plots within this paper and other findings of this study are available from the corresponding author upon reasonable request.

References

37. Kawai, S., Glatzel, T., Koch, S., Baratoff, A. & Meyer, E. Interaction-induced atomic displacements revealed by drift-corrected dynamic force spectroscopy. *Phys. Rev. B* **83**, 035421 (2011).

Acknowledgements

The authors thank V. Speisser for technical support and A. Boeglin and Andrei Borissov for fruitful discussions. This project has received funding from the European Research Council (ERC) under the European Union's Horizon 2020 research and innovation program (grant agreement no. 771850). The Agence National de la Recherche (project SMALL'LED no. ANR-14-CE26-0016-01), the Labex NIE (Contract no. ANR-11-LABX-0058_NIE) and the International Center for Frontier Research in Chemistry (FRC) are acknowledged for financial support. R.S.-M. and H.B. acknowledge GENCI-CINES (Project no. A0060907459) and the Pôle HPC and Equipex Equip@Meso at the University of Strasbourg. T.N. and J.A. acknowledge the project FIS2016-80174-P from the Spanish Ministry of Science, and project ELKARTEK KK-2018/00001 from the Basque Government, as well as grant IT1164-19 from the Basque Government for consolidated groups at the university.

Author contributions

B.D. and G.S. conceived, designed and performed the experiments. B.D., M.R., F.S. and G.S. analysed the experimental data. T.N. and J.A. conceived and performed the simulations of the HRFM maps. R.S.-M. and H.B. performed the density functional theory calculations of the H_2Pc under strain. L.E.P.L. and S.B. performed and analysed the Raman spectra. All the authors discussed the results and contributed to the redaction of the paper.

Competing interests

The authors declare no competing interests.

Additional information

Extended data is available for this paper at https://doi.org/10.1038/s41565-019-0620-x.

Supplementary information is available for this paper at https://doi.org/10.1038/s41565-019-0620-x.

Correspondence and requests for materials should be addressed to G.S.

Peer review information *Nature Nanotechnology* thanks Takashi Kumagai and the other, anonymous, reviewer(s) for their contribution to the peer review of this work.

Reprints and permissions information is available at www.nature.com/reprints.

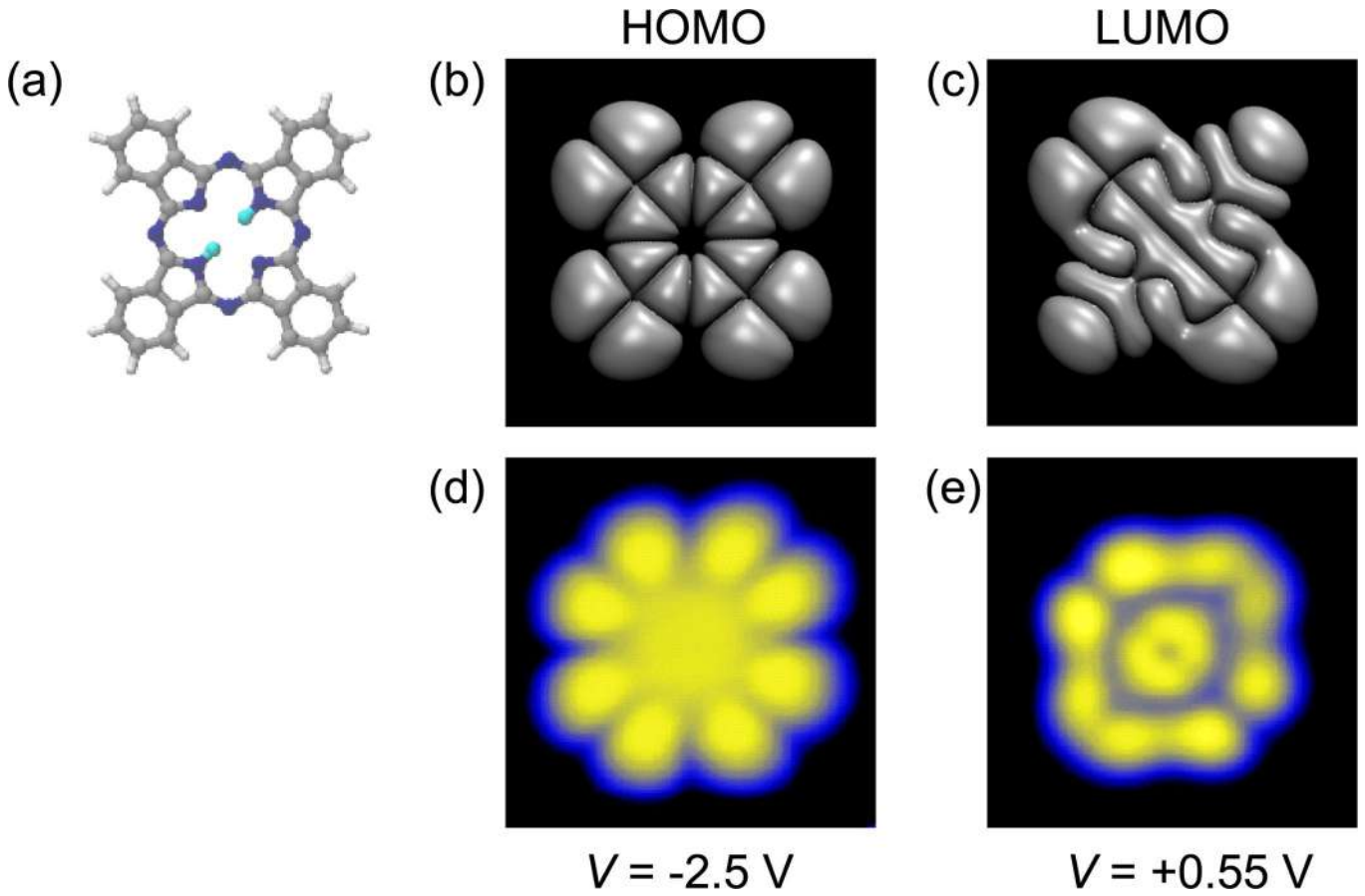

Extended Data Fig. 1 | Experimental and DFT calculated images of the HOMO and LUMO of H_2Pc. a) Chemical structure of free-base phthalocyanine (H_2Pc). DFT calculations (see S5 for details) of the HOMO (**b**) and LUMO (**c**) of H_2Pc, and experimental STM images (**d**, **e**, 3×3 nm^2, $I = 10$ pA) of the same molecular orbitals. This figure corresponds to Fig. S1 of the Supplementary Information.

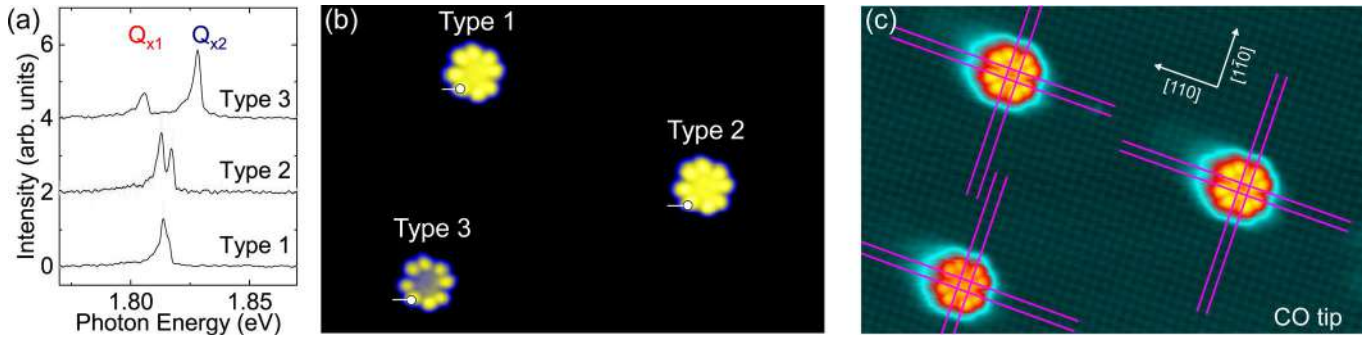

Extended Data Fig. 2 | Spectral split and adsorption site of H_2Pc on NaCl. STM-F spectra acquired at $V = -2.5$ V, $I = 200$ pA, acquisition time t = 300 s for the three different H_2Pc molecules. The spectrum labeled type 1 is similar to the one reported in[14]. STM images (20×14.2 nm^2, $V = -2.5$ V) of the three type of H_2Pc molecules with (**b**) a silver terminated tip and (**c**) a CO terminated tip. The blue lines in (**c**) are aligned with chlorine atomic rows. This figure corresponds to Fig. S2 of the Supplementary Information.

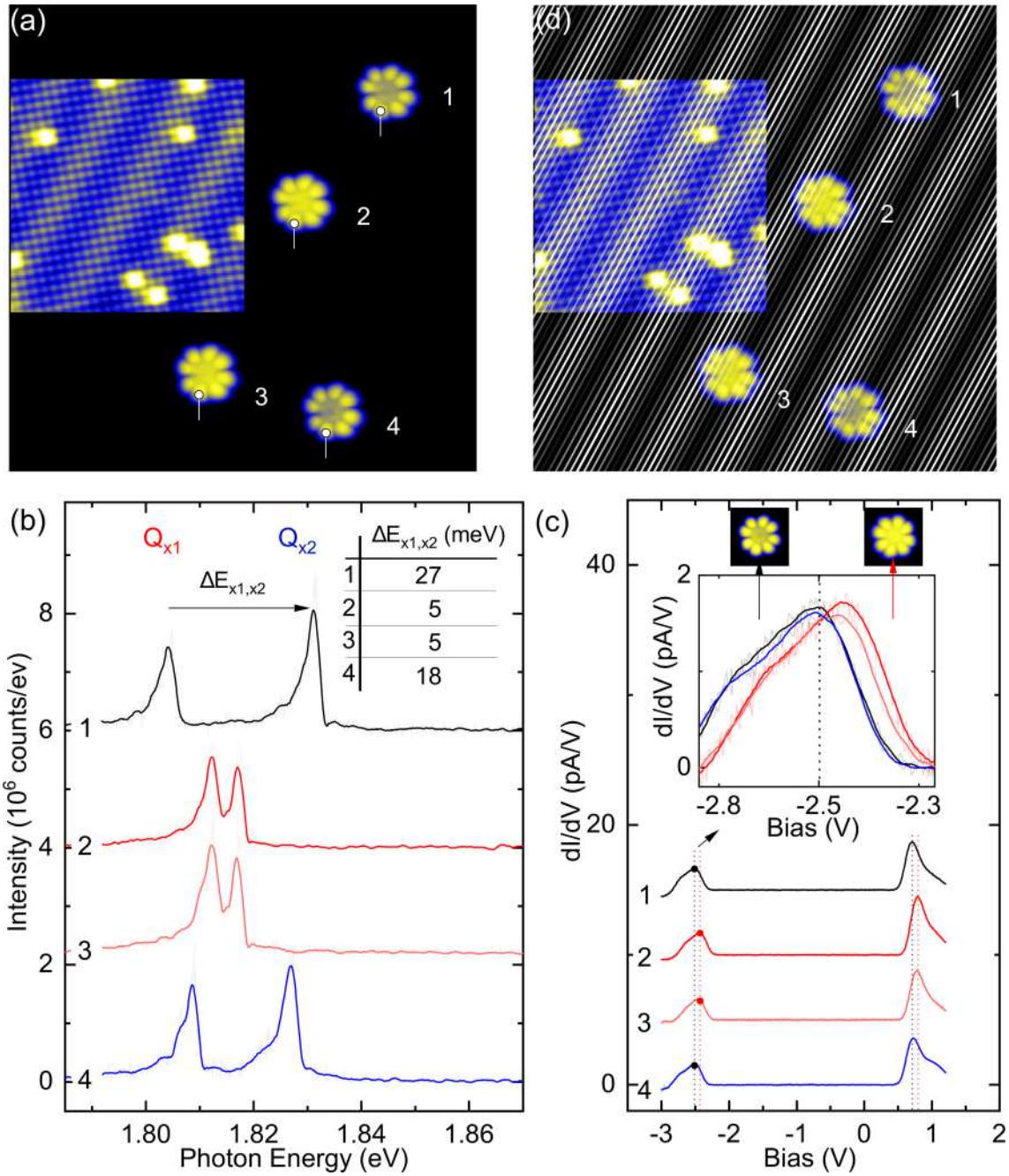

Extended Data Fig. 3 | Effect of the NaCl/Ag(111) Moiré pattern on the electronic and fluorescent properties of adsorbed H_2Pc molecules. a) STM image (20 × 20 m^2, V = –2.5 V) of four H_2Pc molecules. The position of the atomically resolved STM image in inset (10 × 10 nm^2, V = –100 mV) has been precisely adjusted with respect to the larger STM image. (**b**) STM-F spectra acquired at V = –2.5 V, I = 200 pA, acquisition time t = 120 s on the 4 molecules imaged in (**a**). (**c**) d*I*//d*V* spectra acquired on the four molecules imaged in (**a**). (**d**) Same STM image as in (**a**) with an overlaid superstructure of gray lines that follow the linear Moiré pattern. This figure corresponds to Fig. S3 of the Supplementary Information.

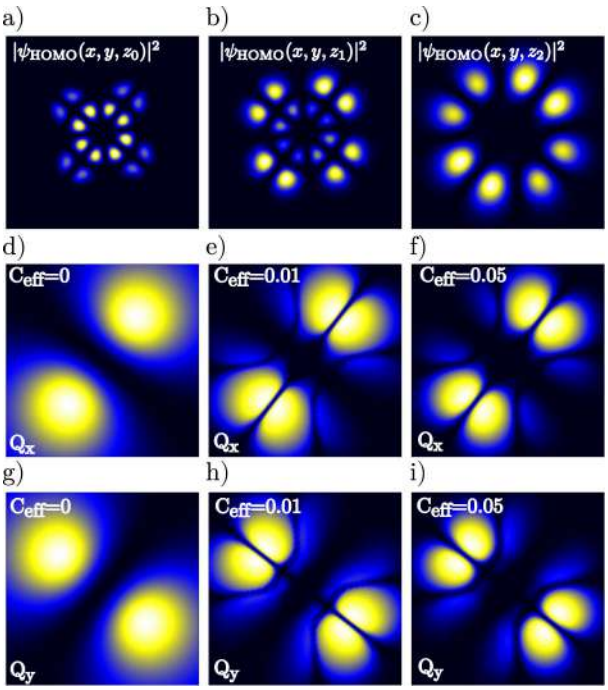

Extended Data Fig. 4 | Calculated photon maps as a function of tip height and tunneling current background. (**a**) Local density of states of the HOMO of the H_2Pc molecule, (**b**,**c**) LDOS of the HOMO for larger distances $z > z_0$ from the plane of the molecule (defined by $z = 0$) propagated until $z_1 = z_0 + 0.2$ nm in (**b**) and $z_2 = z_0 + 0.5$ nm in (**c**). (**d**–**i**) Show normalized photon maps [as given by Eq. (S8)] using the LDOS given in (**c**) for different values of the background current I_{BG} (specified via C_{eff}) for (**d**–**f**) Q_x, and (**g**–**i**) Q_y, respectively. The maps (**d**) and (**g**) calculated assuming $C_{eff} = 0$ are maps of $|g_Q|^2$ as the pumping efficiency η_{exc} (r) is identically equal to one in this case. When $C_{eff} \neq 0$, i.e., a background is considered, the originally smooth broad lobes of the exciton immediately split into smaller lobes as seen in (**e**, **f**, **h**, **i**). This splitting emerges for C_{eff} as small as 0.01 [as shown in (**e**, **h**)]. This figure corresponds to Fig. S4 of the Supplementary Information.

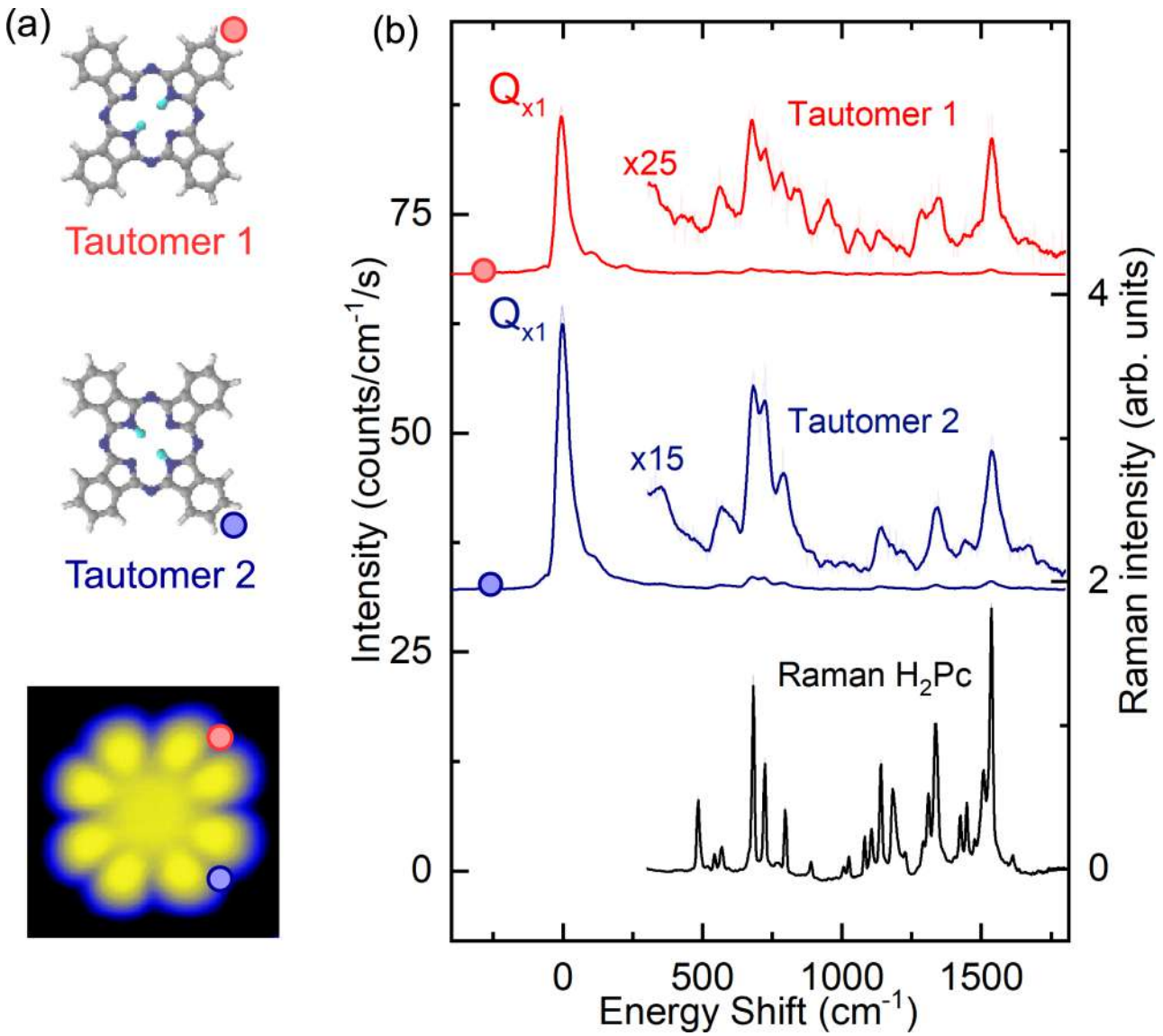

Extended Data Fig. 5 | Vibronic signature of the two tautomers. Vibronic signature of the two tautomers probed by STM-F. We recorded the vibronic spectrum[18] associated to each tautomer. To this end we excited the molecule with the tip located at positions marked by blue and red dots in (**a**), resulting in the preferential emission of one or the other of the tautomers. The obtained vibronic spectra (**b**) can be understood as fingerprints of the molecule in a given environment[18]. As a reference, we also provide a Raman spectrum obtained on a macroscopic crystal of H_2Pc molecules. The vibronic spectrum of tautomer 2 and the Raman spectrum are extremely similar suggesting that tautomer 2 is weakly affected by its adsorption site. The spectrum of tautomer 1, however, reveals important differences, that can hardly be reconciled with the sole modification of the electronic structure of the molecule, but rather indicates modifications of its geometry. This figure corresponds to Fig. S6 of the Supplementary Information.

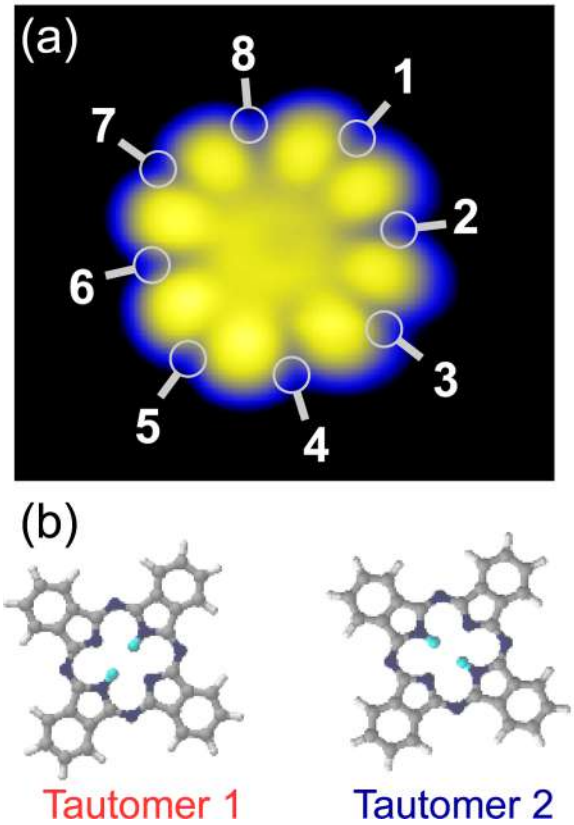

(c)

	Ratio $\alpha = \tau_2/\tau_1$
1	2.5 +/- 0.7
2	1.9 +/- 0.6
3	1.3 +/- 0.2
4	1.4 +/- 0.4
5	2.9 +/- 2
6	1.3 +/- 0.4
7	0.8 +/- 0.3
8	2.2 +/- 0.7

Extended Data Fig. 6 | Ratio of the time spent in each tautomer as a function of tip position. Ratio $\alpha = \tau_2/\tau_1$ of the time spent by the molecule in tautomer 2 and tautomer 1 configurations as a function of the tip position. (**a**) STM image of the molecule ($V = -2.5$ V; $I = 10$ pA). (**b**) Chemical structure of the two tautomers. (**c**) Ratio α of the time spent by the molecule in tautomer 2 and tautomer 1 configurations for the different tip positions marked in (**a**). These values are determined based on 5 s long photon traces recorded simultaneously on APD1 and APD2 at a tunneling current $I = 100$ pA and a bias $V = -2.5$ V following the procedure described in[27]. Except for position 7, the molecule spends always a longer time in the most stable tautomer 2 configuration. The error bars are estimated by accounting for the standard deviation of the averaged light intensity in the bright and dark states of the APD1 and APD2 time traces and the error on the linear fit applied to the correlation functions in logarithmic scale. This figure corresponds to Fig. S9 of the Supplementary Information.

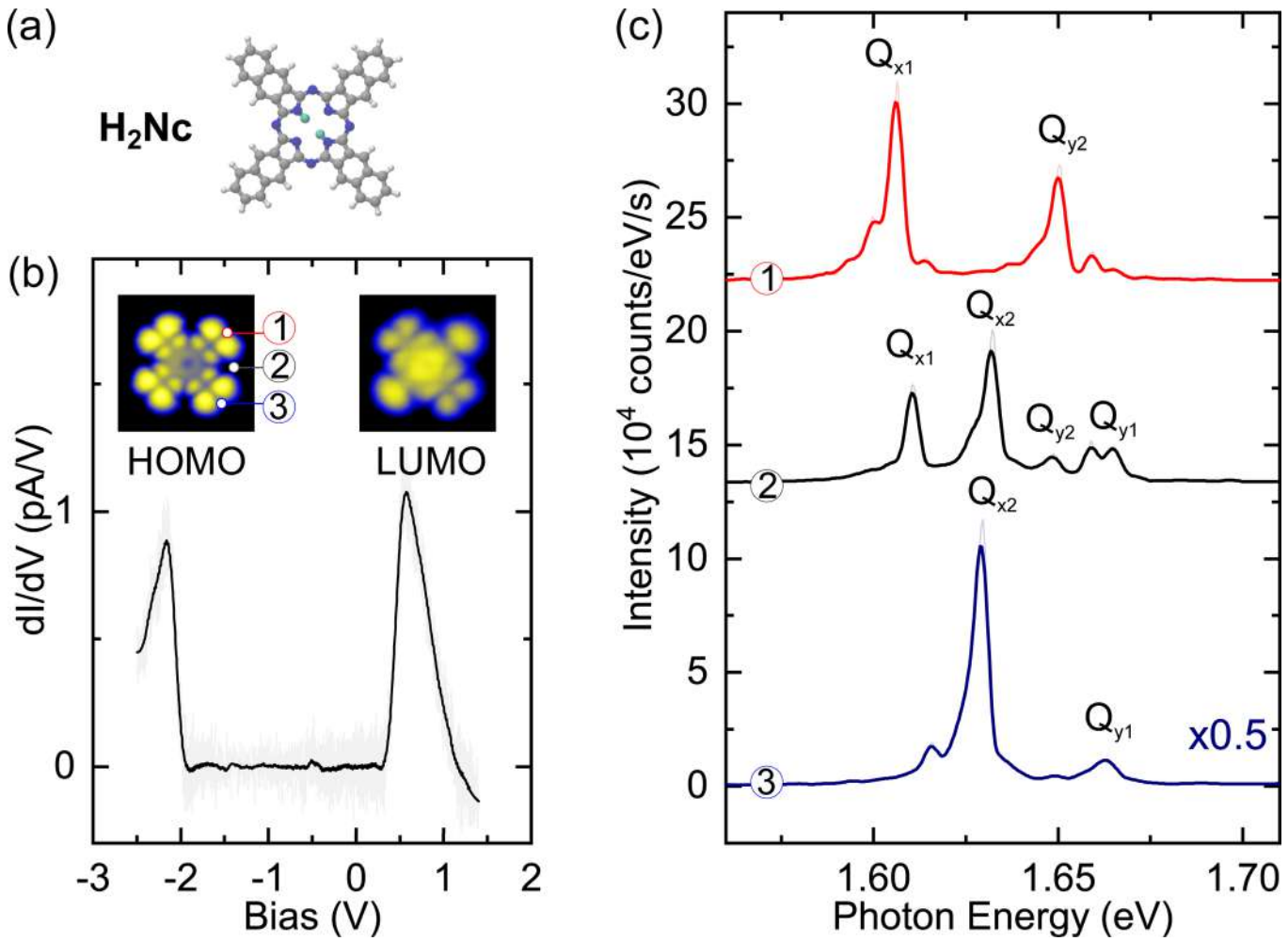

Extended Data Fig. 7 | Electronic and STM-F data on free-base Naphthalocyanine. a) Sketch of the naphthalocyanine molecule (H_2Nc). (**b**) d*I*/d*V* spectrum acquired on a single molecule adsorbed on 3 layers of NaCl on Ag(111). Inset : STM images (3.5 × 3.5 nm^2) of the HOMO ($V = -1.9$ V; $I = 10$ pA) and LUMO ($V = 0.7$ V; $I = 10$ pA). (**c**) STM-F spectra ($V = -2.2$ V; $I = 50$ pA; acquisition time : t = 180 s) acquired with the STM tip located at the positions identified in (**b**). This figure corresponds to Fig. S11 of Supplementary Information.

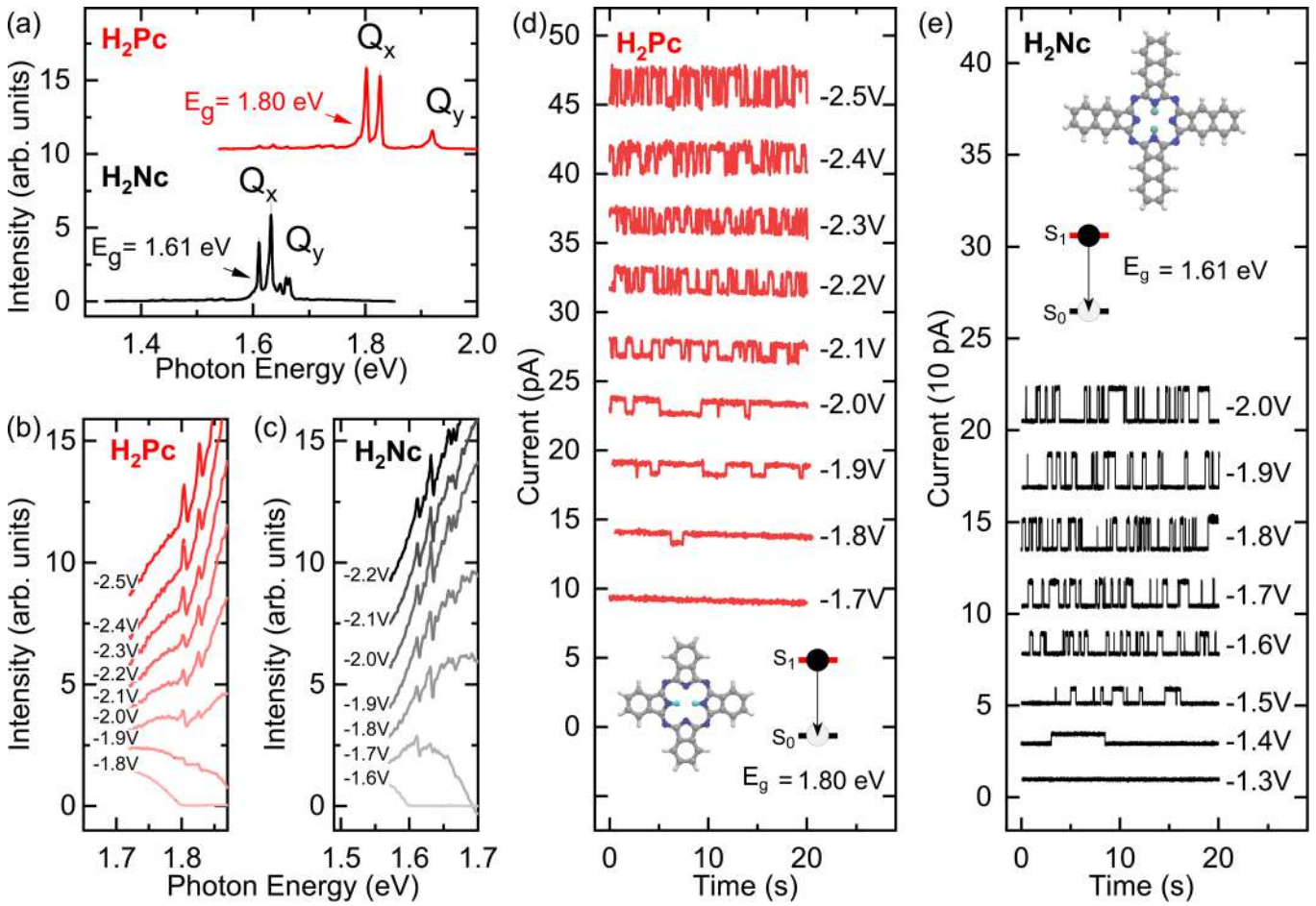

Extended Data Fig. 8 | H_2Pc vs N_2Pc tautomerization onset. (**a**) Comparison between STM-F spectrum of H_2Pc (top spectrum :$V = -2.5$ V; $I = 100$ pA; acquisition time t = 120 s) and H_2Nc (bottom spectrum : $V = -2.2$ V; $I = 50$ pA; acquisition time t = 180 s). (**b**, **c**) At-distance (≈1.2 nm) STM-F spectra as a function of voltage for H_2Pc and H_2Nc ($I = 600$ pA; acquisition time t = 180 s). A vertical offset is used for clarity. (**d**, **e**) Current-time traces (vertically offset for clarity) as a function of voltage for H_2Pc and H_2Nc. An initial setpoint of $I = 10$ pA is used for all traces. The tautomerization voltage onset is very close to the optical gap in both cases, supporting an excited-state mediated tautomerization mechanism. This figure corresponds to Fig. S12 of the Supplementary Information.